An optimisation strategy for the (in- and out-of-plane) resistance of steel beams in demountable composite floor systems

Nijgh, Martin; Veljkovic, Milan

DOI
10.1016/j.istruc.2020.01.049

Publication date
2020

Document Version
Final published version

Published in
Structures

Structures 24 (2020) 880–889

Contents lists available at ScienceDirect

Structures

journal homepage: www.elsevier.com/locate/structures

An optimisation strategy for the (in- and out-of-plane) resistance of steel beams in demountable composite floor systems

Martin Paul Nijgh*, Milan Veljkovic

Faculty of Civil Engineering and Geosciences, Delft University of Technology, Delft, The Netherlands

ARTICLE INFO

Keywords:
Sustainability
Demountable composite floor system
Critical bending moment
Lateral-torsional buckling
Design optimisation

ABSTRACT

Demountable and reusable composite floor systems enable the decoupling between the use of construction materials and economic activity, and hereby contribute to the sustainability of the built environment. Efficient material use through optimised cross-section design reduces construction material demand. Demountable steel-concrete composite floor systems are perceived as competitive when consisting of steel beams and large pre-fabricated concrete floor elements, with composite interaction achieved by demountable shear connectors. Compared to traditional monolithic floor systems, the demountable composite floor systems have an increased sensitivity to lateral-torsional buckling during execution, mostly because of unsymmetrical loading and the absence of rotational constraints in the execution phase. This increased sensitivity implies that the cross-section of the steel beam should not only be designed based on the required in-plane resistance, but should also maximise the out-of-plane resistance. The Energy method and Rayleigh-Ritz methods are combined to develop a prediction model for the critical bending moment of monosymmetrical web-tapered steel beams. The key cross-sectional dimensions and parameters that affect the in-plane and out-of-plane resistance are identified. An overarching strategy for the concurrent optimisation of the in-plane and out-of-plane resistance of mono-symmetrical cross-sections is presented without compromising on material efficiency. The beneficial effects of the proposed optimisation strategy are quantified through a case study example.

1. Introduction

In the coming decades, the global demands for construction materials will double due to a growing global population and a higher standard of living in developing countries [1]. This projection already accounts for beneficial effects such as technological advances in production processes and the change towards a services-based economy. Sustainable existence of humankind is only possible by decoupling economic growth from materials use and environmental impact [2]. The concept of the circular economy aims to facilitate the decoupling by maintaining the highest potential value of materials and products, a strategy first described by Stahel [3]. One of the precursors of the circular economy is Lansink's ladder [4], which prioritises prevention of materials use over mitigating measures, such as reuse and recycling. Sustainable development within the construction sector requires effective ('building the right things') and efficient ('building the things right') materials use. Along these lines, sustainable design methodologies include minimisation of materials use (e.g. design optimisation) and maximisation of structural system reuse [5].

The demountability of bolted connections used in steel structures facilitates reusability of beams and columns, underlining their inherent sustainability potential. Steel is the most recycled material in the world, and its endless recyclability makes it a durable resource [6]. In terms of sustainability, reuse at the level of structural components is prioritised over recycling. The reuse of steel components requires (i) sufficient availability, (ii) a reuse management system, (iii) a stock database, (iv) temporary storage, (v) careful demolition, (vi) acceptance criteria for reuse and (vii) fabrication procedures [7]. Reduction of the material use can be achieved by optimising the steel cross-section design by tapering of the web, which offers both structural and functional advantages, and by a monosymmetrical cross-section design.

Traditional steel-concrete composite floor systems do not facilitate demountability and reusability of the concrete decks or the steel beam, because the structural components are permanently connected by welded headed studs. The development of demountable shear connectors to replace welded headed studs is increasingly gaining attention to enable the transition to a more sustainable construction sector. Experiments to establish the mechanical properties for various types of demountable shear connectors are carried out by, amongst others, Lam et al. [8] and Moynihan & Allwood [9] (bolted headed studs), Wang

* Corresponding author at: Stevinweg 1, 2628 CN, Delft, The Netherlands.
E-mail address: M.P.Nijgh@tudelft.nl (M.P. Nijgh).

https://doi.org/10.1016/j.istruc.2020.01.049
Received 19 November 2019; Received in revised form 30 January 2020; Accepted 31 January 2020

et al. [10] (pretensioned clamping connectors), Pathirana et al. [11] (blind bolts), Suwaed & Karavasilis [12] (precast connector) and Nijgh et al. [13] and Kozma et al. [14] (resin-injected bolted connections). The demountable shear connectors must be sufficiently stiff to generate a significant beneficial effect of the composite interaction to reduce material use by optimising the cross-section area. The material demand can be further reduced by a non-uniform distribution of the shear connectors [13,15,16]. The elastic in-plane behaviour of web-tapered monosymmetrical composite floor systems with non-uniform shear connection can be analysed using the method of Nijgh et al. [17]. Large prefabricated concrete floor elements are favoured over monolithic cast in-situ floors because they increase the reuse potential and facilitate rapid execution and disassembly [13].

Four different design situations are distinguished in EN 1990 [18]: persistent, transient, accidental and seismic design situations. The persistent design situation refers to the conditions of normal use, while the transient design situation refers to temporary conditions, for example execution or repair. During execution, global instability modes may arise in laterally unrestrained steel beams. At a critical load, the compression flange tends to buckle out-of-plane, while the tension flange attempts to maintain the laterally undeformed state of the beam. This causes lateral bending and rotation of the cross-section. This instability phenomenon is known as lateral-torsional or flexural-torsional buckling, and was first theoretically analysed by Prandtl [19] and Michell [20].

The lateral-torsional buckling resistance of a steel beam does not only depend on its cross-sectional properties and support conditions, but also on the detailing of the floor system. Snijder et al. [21] observed that lateral-torsional buckling was prevented by a monolithic concrete floor without mechanical connection to the steel beam, except for a rubber strip ($t = 20$ mm) at the steel-concrete interface. The prevention of lateral-torsional buckling can be attributed to the partially restrained rotation of the cross-section [21,22]. The rotation constraint is caused by a shift of the point of load application from the centre to the tip of the flange, which the only point of contact with the monolithic concrete floor. This constraint is only possible in case of the continuity of the monolithic concrete floor. For a demountable composite floor system, characterised by large discontinuous prefabricated concrete elements, no rotation constraint emerges. The prefabricated floor elements are supported by only one side of the compression flange. The absence of a prefabricated floor element on the other side of the compression flange implies that the cross-section is free to rotate, see Fig. 1. Demountable steel-concrete composite floor systems with discontinuous floor elements are therefore sensitive to lateral-torsional buckling. It should be noted that lateral-torsional buckling is only critical during execution; in the persistent design situation the beam is laterally supported by the concrete floor elements through the demountable shear connectors.

Lateral-torsional buckling can be analysed analytically using equilibrium, energy, and numerical methods [23], although the energy method is most commonly used. The Energy Method is based on the (linear) strain energy of the beam and the work done by the external loads, which are used to evaluate the critical load based on an instability criterion. This method is used for bisymmetrical cross-sections (e.g. [24,25]), for prismatic monosymmetrical cross-sections (e.g. [26–28]), and for web-tapered monosymmetrical cross-sections (e.g. [29–32]), and solved using solution strategies based on the finite element method, finite difference method and Rayleigh-Ritz method.

This paper presents an optimisation strategy to maximise the in-plane and out-of-plane resistances of demountable composite floor systems in the persistent design situation and during execution, respectively. The societal sustainability challenge is addressed by focusing on efficient material use through web-tapered steel beams with monosymmetrical cross-sections, while focusing on minimising the cross-sectional area. The benefits of the proposed design strategy on in-plane and out-of-plane resistances are quantified using a case study example.

2. Prediction model for lateral-torsional buckling

In this section, an analytical prediction method for the critical bending moment of monosymmetrical web-tapered simply-supported steel beams is derived. The proposed model combines the Energy Method approach for web-tapered bisymmetrical cross-sections [24], augmenting it with the effects of monosymmetry and solving it using the Rayleigh-Ritz method. A similar approach was used by Asgarian et al. [31], but in present paper trigonometric instead of power series are used.

The coordinate systems and cross-sectional dimensions used in this paper are illustrated in Fig. 2. The *y-z* coordinate system is used to define the cross-sectional properties, while the *v-w* coordinate system is adopted to describe the out-of-plane and in-plane deflections,

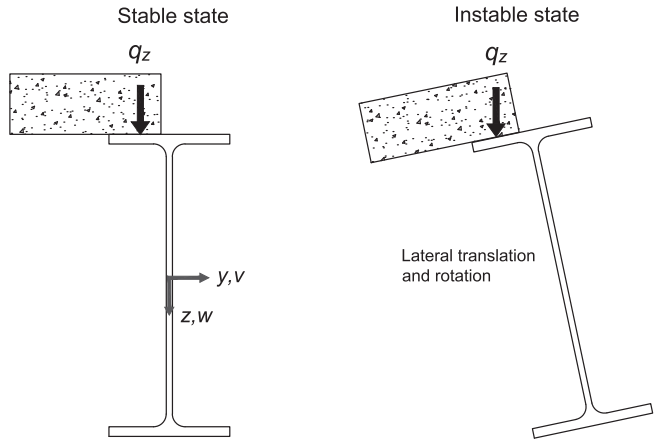

Fig. 1. Sensitivity to lateral-torsional buckling of a steel beam loaded by a prefabricated concrete floor element.

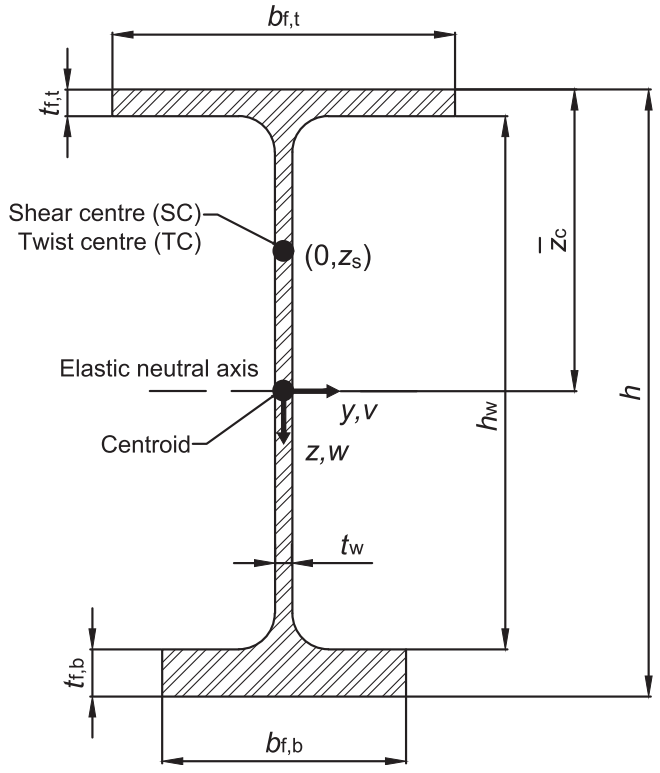

Fig. 2. Axes convention and dimensional parameters for a monosymmetrical cross-section.

respectively. The x-axis is perpendicular to the yz-plane and parallel to the beam span. The cross-sectional dimensions are denoted by b (width), t (thickness) and h (height); the subscripts f and w refer to flange and web, respectively. Distinction between the top and bottom flanges is made by the subscripts t and b, respectively. The total cross-sectional area is denoted by A.

The steel beam is symmetrical in the xz-plane and is subject to loads in positive z-direction. Hence, the beam is subject to uniaxial bending around its strong y-axis prior to the onset of lateral-torsional buckling, with compressive stresses developing above the elastic neutral axis. The y-axis coincides with the elastic neutral axis, and is located at a distance

$$z_c = \frac{b_{f,t}t_{f,t}\left(\frac{t_{f,t}}{2}\right) + h_w t_w\left(t_{f,t} + \frac{h_w}{2}\right) + b_{f,b}t_{f,b}\left(\frac{t_{f,b}}{2} + h_w + t_{f,t}\right)}{A}, \tag{1}$$

from the outer compressive fibre.

Upon reaching a critical load, the cross-section starts to deflect in v-direction and rotates around its twist centre (TC), which coincides with the shear centre (SC) [33,34]. The ordinate of the twist and shear centre is given by

$$z_s = \frac{I_{z,b}}{I_{z,b} + I_{z,t}}\left(h - \frac{t_{f,t}}{2} - \frac{t_{f,b}}{2}\right) + \frac{t_{f,t}}{2} - z_c, \tag{2}$$

with $I_{z,b}$ and $I_{z,t}$ denoting the area moment of inertia around the z-axis of the bottom and top flanges, respectively. The abscissa of the twist and shear centres is at $y_c = 0$.

The cross-sectional parameters (i.e. area, area moment of inertia, torsion rigidity and warping rigidity) depend on the slope α_w of the web proportional to $\cos(\alpha_w)^3$ [24]. The effects of the web-tapering on these cross-sectional parameters are not included in present work because the error for practical web slopes ($\alpha_w < 10\%$) is limited ($< 1.5\%$).

2.1. Strain energy

The prediction of the critical bending moment using the Energy Method requires the determination of the internal strain energy and the virtual work generated by the loads. Relevant contributions to the strain energy originate from [24,26,29,31,32]:

- Normal stresses due to lateral bending around the z-axis
- Shear stresses due to uniform torsion
- Normal stresses due to warping (non-uniform) torsion

The strain energy contributions are superimposed to determine the total internal strain energy. The effects of the pre-buckling deflection along the w-axis are not included in the analysis, because their effects are negligible for typical beam designs ($h/b > 2$) [35,36]. The individual contributions to the internal strain energy are introduced separately in the following subsections.

2.1.1. Strain energy due to lateral bending

Lateral bending induces compressive and tensile stresses in the flanges and web. The end of an infinitesimal beam segment with length dx rotates relative to its other end by a small angle $d\theta$. A bending moment

$$M_z = EI_z\frac{d\theta}{dx} \tag{3}$$

develops, in which EI_z denotes the bending stiffness around the weak axis. The corresponding virtual work of magnitude $dU = 0.5Md\theta$ is stored as strain energy in the beam segment, which can be simplified to

$$dU = \frac{1}{2}\frac{M_z^2}{EI_z}dx. \tag{4}$$

Eq. (4) can be rewritten in terms of lateral deflection and integrated over the beam length to obtain the total strain energy due to lateral bending, given by

$$U_{\text{bending},z} = \frac{1}{2}\int_0^L \left[EI_z\left[\frac{d^2v}{dx^2}\right]^2\right] dx. \tag{5}$$

2.1.2. Strain energy due to uniform torsion

Shear stresses τ_{yz} develop as a result of uniform torsion. The end of an infinitesimal beam segment with length dx rotates relative to its other end by a small angle $d\varphi$. A torque

$$T = GJ_{\text{eff}}\frac{d\varphi}{dx} \tag{6}$$

develops, in which GJ_{eff} denotes the effective torsional rigidity, defined as the sum of the torsional rigidity GJ and the Wagner torsional rigidity β_y. The virtual work of magnitude $dU = 0.5Td\varphi$ is stored as strain energy in the beam segment, which can be simplified to

$$dU = \frac{1}{2}\frac{T^2}{GJ_{\text{eff}}}dx. \tag{7}$$

Eq. (7) can be rewritten in terms of cross-sectional rotation and integrated over the beam length to obtain the total strain energy due uniform torsion, given by

$$U_{\text{uniform torsion}} = \frac{1}{2}\int_0^L \left[GJ_{\text{eff}}\left[\frac{d\varphi}{dx}\right]^2\right] dx. \tag{8}$$

2.1.2.1. Torsional rigidity. The effective torsional rigidity GJ_{eff} is the sum of the torsional rigidity GJ and the Wagner torsional rigidity β_y. The free torsional rigidity is the product of the shear modulus G and the torsional constant J, defined as

$$J = \xi_{f,t}b_{f,t}t_{f,t}^3 + \xi_w h_w t_w^3 + \xi_{f,b}b_{f,b}t_{f,b}^3, \tag{9}$$

in which ξ is a correction factor depending on the aspect ratio of the flange or web. For thin-walled parts ($b/t > 10$) ξ may be taken as 1/3.

2.1.2.2. Wagner torsional rigidity. The Wagner torsional rigidity β_y originates from compressive and tensile bending stresses which form a resulting torque in case of monosymmetrical cross-sections. The Wagner torsional rigidity has a significant potential to optimise the critical bending moment; its effect was first recognised by Kerensky, Flint and Brown [37] and later refined by Nethercot and Taylor [38]. The expression for the Wagner torsional rigidity is often included in literature, without identifying the true source of this term (e.g. in [27,28,39,40]). Its derivation is included in present work to illustrate its potential benefits to optimise the critical bending moment for a given cross-sectional area.

The Wagner torque β_y is derived by assuming that the end of infinitesimal segment dx of a monosymmetrical cross-section is subject to a rotation $d\varphi$ with respect to its other end, see Fig. 3. This causes a differential displacement of cross-sectional elements at infinitesimal distance dx. Using the small angle approximation, the displacement of each cross-sectional element perpendicular to the line connecting the centroid of the cross-sectional element and the twist centre (TC), is given by

$$\delta = a\cdot d\varphi = \sqrt{(z - z_s)^2 + (y - y_s)^2}\cdot d\varphi. \tag{10}$$

The inclination between the cross-sectional elements at both ends of the infinitesimal segment dx equals

$$\delta' = a\cdot\frac{d\varphi}{dx}. \tag{11}$$

Consequently, the normal stresses $\sigma_\parallel$ (parallel to the beam axis) due to bending generate a stress component $\sigma_\perp$ perpendicular to the line connecting the centroid of the cross-sectional element and the twist centre, see Fig. 4. The magnitude of this stress component is

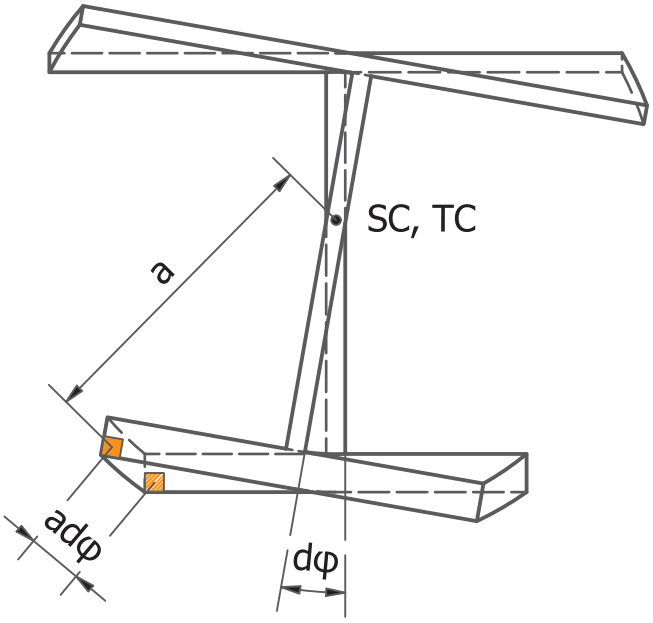

Fig. 3. Torsion of a monosymmetrical cross-section leading to a rotation dφ around the shear centre and a displacement adφ of the cross-sectional elements.

$$\sigma_{\perp} = \sigma_{\parallel} a \cdot \frac{d\varphi}{dx}. \tag{12}$$

The stress components generate a bending moment around the twist centre with a magnitude

$$dM = \sigma_{\perp} a \cdot dA = \sigma_{\parallel} a^2 \cdot dA \cdot \frac{d\varphi}{dx}. \tag{13}$$

The resulting torque around the twist centre generated by the cross-section is then given by

$$T = \int dM = \frac{d\varphi}{dx} \int_A \sigma_{\parallel} a^2 dA = \beta_y \frac{d\varphi}{dx}, \tag{14}$$

which stiffens the torsional response if positive. In Eq. (14) $\beta_y = \int_A \sigma_{\parallel} a^2 dA$ is introduced as the Wagner torsional rigidity. For monosymmetrical beams subject to bending solely around the strong y-axis, β_y can be expressed by

$$\beta_y = \frac{M_y}{I_y}\left(\int_A y^2 z dA + \int_A z^3 dA\right) + 2z_s, \tag{15}$$

Eq. (15) demonstrates that the Wagner torsional rigidity is positive ($\beta_y > 0$) if the tension flange (positive z-direction) is further from the shear centre than the compression flange. Similarly the Wagner torsional rigidity is negative if the compression flange is further from the shear centre compared to the tensile flange. For bisymmetrical cross-sections it follows that $\beta_y = 0$ and thus $GJ_{\text{eff}} = GJ$.

2.1.3. Strain energy due to warping torsion

Zhang & Tong [24] derived the linear strain energy related to warping torsion of a web-tapered I beam undergoing lateral torsional buckling as

$$U_{\text{warping torsion}} = \frac{1}{2}\int_0^L \left[EI_\omega \left[\frac{\mathrm{d}^2\phi}{\mathrm{d}x^2}\right]^2 + 2\frac{\mathrm{d}^2 EI_\omega}{\mathrm{d}x^2}\left[\frac{\mathrm{d}\phi}{\mathrm{d}x}\right]^2 + 2\frac{\mathrm{d}EI_\omega}{\mathrm{d}x}\frac{\mathrm{d}\phi}{\mathrm{d}x}\frac{\mathrm{d}^2\phi}{\mathrm{d}x^2}\right] \mathrm{d}x. \tag{16}$$

The latter two terms in Eq. (16) represent the effects originating from the non-prismatic (tapered) geometry of the beam. The warping rigidity I_ω is expressed as

$$I_\omega = \frac{I_{z,\mathrm{b}} I_{z,\mathrm{t}}}{I_{z,\mathrm{b}} + I_{z,\mathrm{t}}}\left(h - \frac{t_{\mathrm{f,t}}}{2} - \frac{t_{\mathrm{f,b}}}{2}\right)^2, \tag{17}$$

in which $I_{z,\mathrm{b}}$ and $I_{z,\mathrm{t}}$ denote area moment of inertia around the z-axis of the bottom and top flanges, respectively.

2.1.4. Total strain energy

The total linear strain energy U associated with the lateral-torsional buckling of a web-tapered I-section is determined by combining Eqs. (5), (8), and (16), resulting in

$$U = \frac{1}{2}\int_0^L \left[EI_z\left[\frac{d^2v}{dx^2}\right]^2 + \left(GJ + \beta_y + 2\frac{d^2 EI_\omega}{dx^2}\right)\left[\frac{d\phi}{dx}\right]^2 + EI_\omega\left[\frac{d^2\phi}{dx^2}\right]^2 + 2\frac{dEI_\omega}{dx}\frac{d\phi}{dx}\frac{d^2\phi}{dx^2}\right] dx. \tag{18}$$

Eq. (18) is identical to the linear strain energy derived by Zhang & Tong [24], except for the Wagner torsional rigidity term, which was not included because their work focused on bisymmetrical tapered beams.

2.2. Virtual work of the loads

Possible loads in z direction include uniformly distributed loads q_z and concentrated loads P_z, which are applied in the plane of symmetry at ordinates z_q and z_P, respectively. The vertical displacement of the external loads due to the rotation of the cross-section generates virtual work. The loads and vertical displacement act in the same direction if

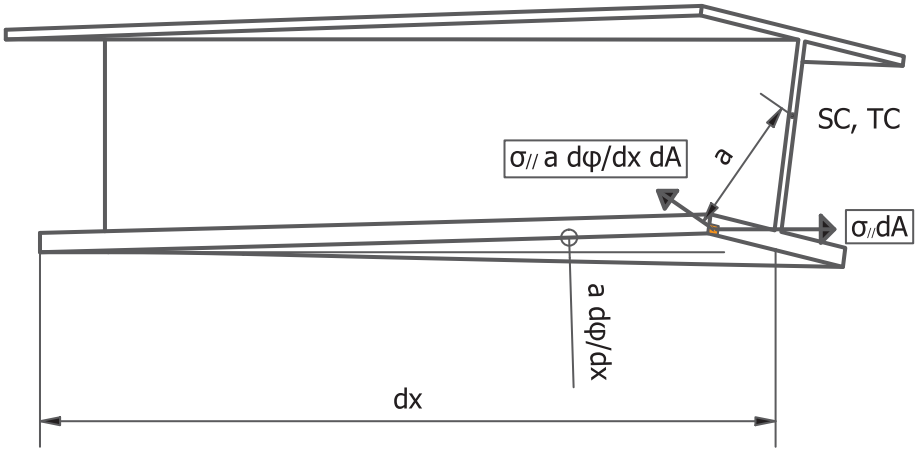

Fig. 4. The relative inclination of the flanges causes the longitudinal stresses $\sigma_{\parallel}$ to generate a stress component perpendicular to the line connecting the centroid of the cross-sectional element and the twist centre.

the loads are applied above the shear centre. This leads to positive virtual work, reducing the critical lateral-torsional buckling load. Applying the loads below the level of the shear centre increases the critical lateral-torsional buckling load. Additional virtual work is generated by the bending moment M_y, resulting from q_z and P_z, subject to the rotation $\varphi(x)$ of the cross-section of the beam.

The total virtual work generated by the external loads can be expressed by [41]:

$$V = \int_0^L \left[M_y \varphi \frac{\mathrm{d}^2 v}{\mathrm{d}x^2} - \frac{1}{2} q_z (z_\mathrm{s} - z_\mathrm{q}) \varphi^2 \right] \mathrm{d}x - \frac{1}{2} \sum P_z (z_\mathrm{s} - z_\mathrm{P}) \varphi^2_{x=x\mathrm{P}}. \tag{19}$$

2.3. Total internal energy

By the principle of conservation of energy, the total work done by the loads must be balanced by the internal strain energy. The total energy of the beam equals

$$\prod = U - V \tag{20}$$

The conservative elastic system is in a state of stable equilibrium if, and only if, the value of the potential energy is a relative minimum. This means that the onset of lateral-torsional buckling is characterised by a stationary condition of the total energy function, such that the derivative of Eq. (20) must be zero.

2.4. Solution strategy

The deformation functions $v(x)$ and $\varphi(x)$ in Eqs. (18) and (19) are unknown. The lateral-torsional eigenmodes of the beam can be approximated by the Rayleigh-Ritz method. This method is based on the assumption that the deformation functions can be approximated by a linear combination of a number of independent linear functions. The independent functions must satisfy the boundary conditions and any intermediate restraints.

For a simply-supported beam without any intermediate lateral restraints, the lateral deflection $v(x)$ can be approximated by the following function [32]:

$$v = \sum_{m=1}^{n} c_{v,m} \sin\left(m \frac{\pi x}{L}\right), \tag{21}$$

where $c_{v,m}$ is a weighing factor of lateral deflection mode m. Similarly, the rotation field $\phi(x)$ of a simply-supported beam with fork supports (restraining motion along the y-axis and rotation around the x-axis) can be approximated by:

$$\varphi = \sum_{m=1}^{n} c_{\varphi,m} \sin\left(m \frac{\pi x}{L}\right). \tag{22}$$

The assumed lateral deflection and rotation fields discretise the problem in $2(n - m + 1)$ degrees of freedom. In case other supports or restraints are present, Eqs. (21) and (22) must be modified accordingly. For example, $m = 2$ for a simply-supported beam with a lateral and torsional restraint at mid-span. The number of modes n must (i) be as small as possible to minimise the computational time and (ii) be as large as required to obtain satisfactory results. The number of modes n is determined based on a sensitivity study; the results obtained with n modes must convergence to the result for $n \to \infty$ modes.

Eqs. (21) and (22) are substituted in the total energy function given by Eq. (20). The onset of lateral-torsional buckling is characterised by a stationary condition of the total energy function, implying that

$$\frac{\partial \prod}{\partial c_{\varphi,m}} = \frac{\partial \prod}{\partial c_{v,m}} = 0, \tag{23}$$

representing a local minimum for the potential energy function for each of the $2(n - m + 1)$ degrees of freedom. Eq. (23) leads to a linear system of $2(n - m + 1)$ equations, which can be represented in matrix form as

$$[A][c] = 0, \tag{24}$$

where A is the coefficient matrix and c is a column vector containing the unknown variables $c_{\varphi,m}$ and $c_{v,m}$. The coefficient matrix A solely depends on the unknown critical load $q_{z,\mathrm{cr}}$ and/or $P_{z,\mathrm{cr}}$. Non-trivial solutions only exist if $\det[A] = 0$. Solving this equation gives the eigenvalues of the coefficient matrix. The critical load can be determined by multiplying the magnitude of the imposed loads q_z and/or P_z by the smallest positive eigenvalue; the larger eigenvalues represent higher-order lateral-torsional buckling modes.

2.5. Validation

The method outlined above is validated by comparing its results against outcomes reported in literature. The work of Asgarian et al. [31] and Andrade et al. [32] is selected for the validation of the prediction model.

2.5.1. *Asgarian et al.* [31]

Asgarian et al. [31] investigated the lateral-torsional buckling of simply-supported mono- and bisymmetrical tapered beams subject to uniformly distributed loads q_z using the finite element method. The span ranges from $L = 6 - 10$ m and the beams are symmetric with respect to the *y,z*-plane at midspan. The external load is either applied on the top flange or at the shear centre. The tapering of the web is introduced through α, defined as the ratio of the beam height at the support ($h_{\min}$) over the beam height at midspan ($h_{\max}$). The cross-sections considered have the following dimensional properties:

- Monosymmetrical cross section:

$h_{\max} = 300$ mm ; $h_{\min} = \alpha h_{\max}$; $b_{\mathrm{f,t}} = 150$ mm ; $b_{\mathrm{f,b}} = 75$ mm ; $t_{\mathrm{f,t}} = t_{\mathrm{f,b}} = 10.7$ mm ; $t_\mathrm{w} = 7.1$ mm

- Bisymmetrical cross section:

$h_{\max} = 300$ mm ; $h_{\min} = \alpha h_{\max}$; $b_{\mathrm{f,t}} = b_{\mathrm{f,b}} = 150$ mm ; $t_{\mathrm{f,t}} = t_{\mathrm{f,b}} = 10.7$ mm ; $t_\mathrm{w} = 7.1$ mm

The results of the proposed method are compared to the finite element results reported by Asgarian et al. [31] in terms of the critical bending moment $M_\mathrm{cr} = 0.125 q_{z,\mathrm{cr}} L^2$. The number of Rayleigh-Ritz modes n is 7 based on a sensitivity study. The critical bending moments corresponding to uniformly distributed loads applied on the top flange ($z_q = -z_\mathrm{c}$) and applied at the level of the shear centre ($z_q = z_\mathrm{s}$) are presented in Tables 1 and 2, respectively. Good agreement between the analytical and finite element modelling strategies is observed, particularly for longer span beams. Substantial tapering and short beam spans lead to slightly larger differences, which is attributed to web distortion and compression flange distortion [32]. The former is characterised by lateral bending of the web, the latter by in-plane bending of the compression flange and the associated non-perpendicularity of the flange with respect to the web.

2.5.2. *Andrade et al.* [32]

Andrade et al. [32] investigated the lateral-torsional buckling of simply-supported bisymmetrical tapered beams subject to concentrated loads P_z using the finite element method. The span ranges from $L = 6 - 12$ m and the beams are symmetric with respect to the *y,z*-plane at midspan. The external load is either applied on the top flange or at the shear centre. The tapering of the web is introduced through parameter α, indicating the relative beam height at the support ($h_{\min}$) compared to midspan ($h_{\max}$). The cross-section considered has the

Table 1
Comparison between results obtained using present method and finite element results by Asgarian et al. [31] for load application on the top flange.

L (m)	α (–)	Bisymmetrical cross-section			Monosymmetrical cross-section		
		M_{cr}(kNm)		Deviation (%)	M_{cr}(kNm)		Deviation (%)
		Present method	Asgarian et al. [31]		Present method	Asgarian et al. [31]	
6	0.6	61.04	58.4	4.52	55.11	54.01	2.04
	0.8	64.53	62.5	3.25	58.53	57.14	2.43
	1.0	70.61	70.58	0.04	62.68	62.73	−0.08
8	0.6	46.55	45.4	2.53	39.94	41.06	−2.73
	0.8	48.16	47.46	1.47	41.88	41.80	0.19
	1.0	51.06	51.31	−0.49	44.14	44.31	−0.38
10	0.6	37.9	37.3	1.61	31.31	31.68	−1.17
	0.8	38.82	38.4	1.09	32.61	31.95	2.07
	1.0	40.48	40.77	−0.71	34.07	34.31	−0.70

following dimensional properties:

$h_{max} = 600$ mm ; $h_{min} = \alpha h_{max}$; $b_{f,t} = b_{f,b} = 150$ mm ; $t_{f,t} = t_{f,b} = 12.7$ mm ; $t_w = 9.5$ mm

The results of the proposed method are compared to the finite element results reported by Andrade et al. [32] in terms of the critical bending moment $M_{cr} = 0.25 P_{z,cr} L$. The number of Rayleigh-Ritz modes n is 7 based on a sensitivity study. The critical bending moments are presented in Table 3. Good agreement between the analytical and finite element modelling strategies is observed, again the deviations are larger for more pronounced tapering ratios and shorter beam spans.

3. Generic lateral-torsional buckling design verification according to Eurocode 3

Eurocode 3 contains a generic method that should be applied to determine the lateral torsional buckling design resistance of non-prismatic members. It must be verified that

$$\frac{\chi_{op}\alpha_{ult,k}}{\gamma_{M1}} \geqslant 1.0, \tag{25}$$

in which χ_{op} is a reduction factor related to lateral torsional buckling and $\alpha_{ult,k}$ is the minimum load amplifier of the design loads such that the characteristic in-plane resistance of the cross section is attained. A load amplification factor $\alpha_{cr,op}$ is introduced, which is the ratio of the critical bending moment M_{cr} over the design bending moment $M_{y,Rd}$. According to the Dutch National Annex [42] to EN 1993-1-1 [43], $\alpha_{cr,op}$ should be determined based on the effective critical bending moment $M^*_{cr} = k_{red} M_{cr}$ to account for the effects of web distortion. The reduction factor k_{red} is defined as

$$k_{red} = \begin{cases} 1 & h/t_w \leqslant 75 \\ \min(1.03 - 5.4\cdot10^{-5}\alpha,\ 1) & h/t_w > 75,\ \alpha \leqslant 5000, \end{cases} \tag{26}$$

with

$$\alpha = \frac{h t_f \cdot 10^{12}}{t_w^3 b L_g^2} > 575. \tag{27}$$

Based on the load amplification factors, the global non-dimensional slenderness for the beam element is defined as

$$\bar{\lambda}_{op} = \sqrt{\frac{\alpha_{ult,k}}{\alpha_{cr,op}}}. \tag{28}$$

The reduction factor for lateral-torsional buckling χ_{op} is expressed by

$$\chi_{op} = \min\left(\frac{1}{\Phi_{op} + \sqrt{\Phi_{op}^2 - \bar{\lambda}_{op}^2}}, 1\right), \tag{29}$$

with

$$\Phi_{op} = 0.5[1 + \alpha_{LT}(\bar{\lambda}_{op} - 0.2) + \bar{\lambda}_{op}^2], \tag{30}$$

where α_{LT} is an imperfection factor for lateral torsional buckling, and depends on the height over width ratio and the type of cross section. After determining the reduction factor χ_{op} the design verification for lateral torsional buckling can be carried out through Eq. (25).

4. Optimisation of in-plane and out-of-plane resistance

Eq. (25) includes the coupling between the in-plane and out-of-plane resistance of a beam. Designing a cross-section that maximises the in-plane and out-of-plane resistances contributes to the material

Table 2
Comparison between results obtained using present method and finite element results by Asgarian et al. [31] for load application at the shear centre.

L (m)	α (–)	Bisymmetrical cross-section			Monosymmetrical cross-section		
		M_{cr}(kNm)		Deviation (%)	M_{cr}(kNm)		Deviation (%)
		Present method	Asgarian et al. [31]		Present method	Asgarian et al. [31]	
6	0.6	81.71	79.64	2.60	58.98	60.23	−2.08
	0.8	86.41	85.21	1.41	62.72	65.85	−4.75
	1.0	94.02	92.32	1.84	67.17	66.23	1.42
8	0.6	58.54	57.86	1.18	42.06	43.37	−3.02
	0.8	60.84	60.65	0.31	44.17	43.30	2.01
	1.0	64.43	63.9	0.83	46.58	46.34	0.52
10	0.6	45.72	45.46	0.57	32.64	32.21	1.33
	0.8	47.11	47.07	0.08	34.04	34.83	−2.27
	1.0	49.2	48.98	0.45	35.59	35.47	0.34

Table 3
Comparison between results obtained using present method and finite element results by Andrade et al. [32]

L (m)	α (–)	Load on top flange			Load at shear centre		
		M_{cr}(kNm)		Deviation (%)	M_{cr}(kNm)		Deviation (%)
		Present method	Andrade et al. [32]		Present method	Andrade et al. [32]	
6	0.6	108.1	103.8	4.14	176.8	168.5	4.90
	0.8	124.8	124.9	−0.08	196.7	190.1	3.47
	1.0	147.8	149.0	−0.74	223.3	211.9	5.40
12	0.6	56.33	56.25	0.14	76.06	75.96	0.13
	0.8	60.10	60.60	−0.83	80.30	80.61	−0.38
	1.0	65.06	65.76	−1.06	85.76	86.01	−0.29

efficiency. In this section, a strategy for the optimisation of in-plane and out-of-plane resistance is presented.

4.1. Optimisation of the out-of-plane resistance

The out-of-plane resistance of a demountable composite floor system is only relevant during the execution of the demountable composite floor system. The prefabricated concrete floor elements must be positioned on the top flange to ensure an even and continuous surface of the floor system. Previously, it was shown that the position of the shear centre has a significant effect on the effective torsional rigidity because of the contribution of the Wagner torsional rigidity; the effect is beneficial if the compression flange is closest to the shear centre. According to Eq. (2), the location of the shear centre is closest to the compression flange if

$$\frac{I_{z,b}}{I_{z,b} + I_{z,t}} = 0, \tag{31}$$

implying that a T-shaped cross-section maximises the Wagner torsional rigidity. A T-shaped section implies that the warping rigidity is zero. However, the effects of the increased effective torsional rigidity are generally dominant over the reduction of the warping rigidity, resulting in an increase of the critical bending moment for the same cross-sectional area A.

4.2. Optimisation of the in-plane resistance

The in-plane resistance of a demountable composite floor system is relevant both during execution and in the persistent design situation. The reuse of the steel beam is only possible if no plastification of any part of the cross-section has occurred [44], implying that nowhere in the cross-section the yield strength f_y may be exceeded. Normal stresses in the beam originate from the self-weight of the beam and the floor elements (imposed during execution) and the live-load, carried through composite interaction in the persistent design situation. The magnitude of the normal stresses must be approximately equal in tension and compression to optimise the in-plane resistance. This implies that the elastic neutral axis of the steel beam must be located at or below mid-height of the cross-section, depending on the relative contribution of the loads imposed during the execution and the persistent design situation.

The beneficial effect of composite interaction in the persistent design situation depends, among other parameters, on the square of the distance between the elastic neutral axes of the steel beam and the prefabricated concrete floor elements. The requirements of the execution and persistent design situations with respect to the location of the elastic neutral axis are therefore aligned.

4.3. Concurrent optimisation of the in-plane and out-of-plane resistance

The optimal design to maximise the in-plane and out-of-plane resistance minimises $I_{z,b}$, locates the elastic neutral axis at approximately mid-height of the cross-section and leads to a sufficiently high area moment of inertia I_y. These demands can be accomplished by designing a monosymmetrical cross-section subject to the following constraints:

$$I_{z,b} \ll I_{z,t} \;\; \therefore \;\; b_{f,b} \ll \sqrt[3]{\frac{t_{f,t} b_{f,t}^3}{t_{f,b}}},$$
$$t_{f,t} b_{f,t} \approx t_{f,b} b_{f,b}. \tag{32}$$

This strategy ensures (i) maximisation of the out-of-plane resistance during execution, (ii) an optimal stress distribution over the height of the cross-section during execution and in the persistent design situation, and (iii) a significant effect of the shear interaction in the persistent design situation. The dimensions of the top flange can be determined first, e.g. based on cross-section classification limits or based on practical considerations, for example the minimum width needed to support the prefabricated concrete floor elements. The area of the bottom flange must be approximately equal to that of the top flange whilst minimising the bottom flange width within practical limitations, such as the availability of thick plate material. The fabrication process of the optimised cross-section requires the availability of equipment to align both flanges with the centreline of the web.

5. Case study

The beneficial effects of the proposed cross-section design strategy are demonstrated through a case study example of a demountable composite floor system with a clear span of 16 m. The simply-supported demountable composite floor system consists of web-tapered steel beams and large prefabricated concrete floor (8 × 2.6 × 0.12 m) elements, see Fig. 5. The demountable shear connectors with stiffness k_{sc} = 55 kN/mm [13] are assumed to be concentrated near the supports, where their beneficial influence is largest [13,15–17,45]. Eight pairs of connectors are uniformly distributed between the supports and a distance $L/10$ from the supports. In the remaining part of the span, the shear connectors are widely spaced at a centre-to-centre distance of $L/10$.

The steel beam of steel grade S355 has a height of h = 590 mm at the supports and h = 740 mm at mid span. The starting point for the design is that the top and bottom flanges are identical: $t_{f,t} = t_{f,b}$ = 12 mm and $b_{f,t} = b_{f,b}$ = 300 mm. Two design cases are considered: (i) the dimensions of the top flange are fixed (300 × 12 mm^2) and the bottom flange dimensions are varied, and (ii) the dimensions of the bottom flange are fixed (300 × 12 mm^2) and the top flange dimensions are varied. The variation of the flange dimensions is constrained to the condition that the area of the top and bottom flanges are equal, i.e. $t_{f,t} b_{f,t} = t_{f,b} b_{f,b}$. The web thickness is kept constant as t_w = 4.5 mm.

The design value of the self-weight of the steel beam and the floor elements is $q_{z,G,Ed}$ = 12 kN/m, imposed during the execution and therefore carried solely by the steel beam. It is conservatively assumed that the self-weight of the floor elements acts on both the left and right side of the upper flange and that potentially favourable effects (e.g.

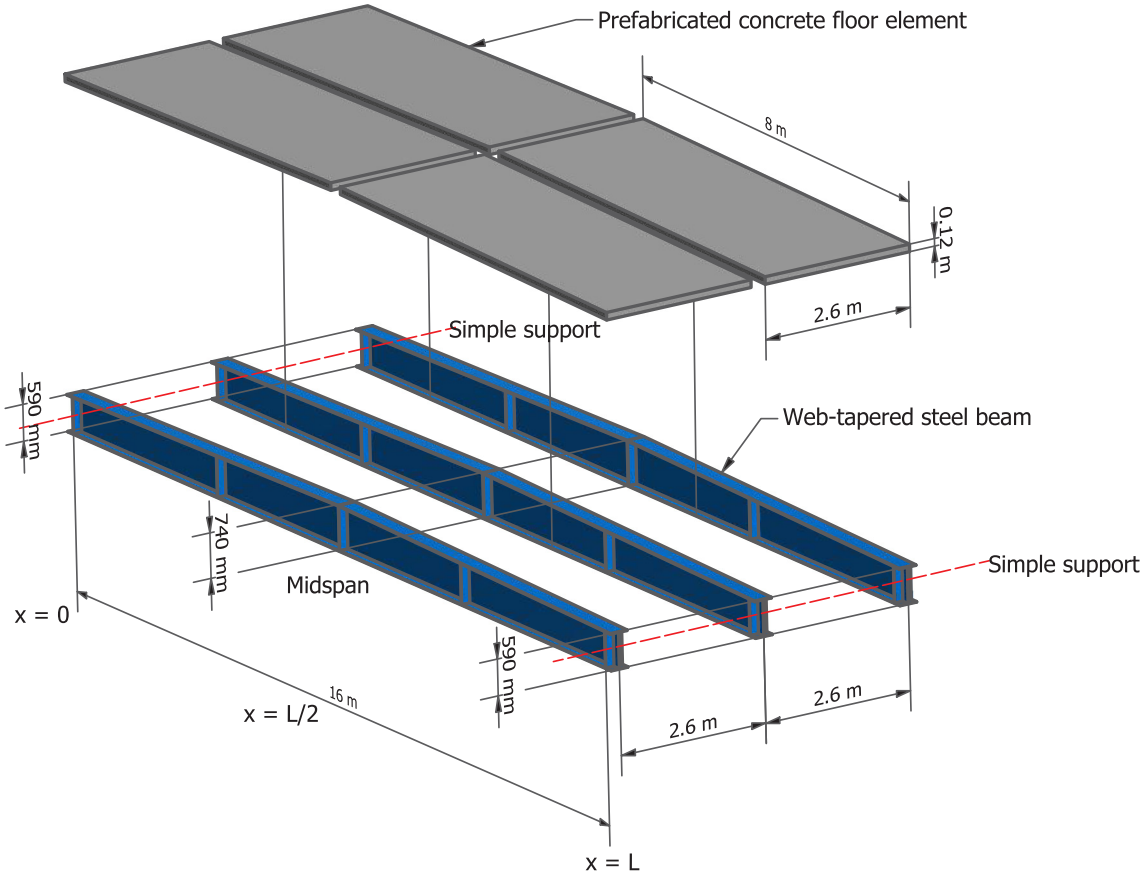

Fig. 5. A repetitive characteristic part of the case study composite floor system, consisting of simply supported web-tapered beams and prefabricated concrete floor elements. Rotation of the cross-section is prevented at the supports. For the braced alternative, rotation and lateral displacement at midspan is also prevented.

friction, bending stiffness) do not restrain the out-of-plane motion and rotation of the beam. Two lateral support conditions are considered during execution: (i) laterally unsupported and (ii) laterally supported by a bracing system at midspan. In both cases rotation of the cross-section around the *x*-axis is prevented at the supports. In the persistent design situation any out-of-plane deformation is constrained by the demountable shear connectors. The design value of the live load, expected in a multi-storey car park building [18], imposed during the persistent design situation is $q_{z,Q,Ed} = 11.7$ kN/m.

The design values of the loads are used to determine the resistances, while their characteristic values $q_{z,G,Ek} = q_{z,G,Ed}/1.35$ and $q_{z,Q,Ek} = q_{z,Q,Ed}/1.5$ are used for the serviceability limit state. The deflection and stresses during the execution are determined based on Euler-Bernoulli beam theory, while their magnitudes in the persistent design situation are determined based on the model of Nijgh & Veljkovic [17].

Fig. 6 illustrates the critical bending moment and the total deflection (due to self-weight and live load) for the scope of cross-section designs. Cross-sections with $b_{f,b}/b_{f,t}$ ratios < 1 generate the highest critical bending moment. Within the case study boundaries, the maximum critical bending moment is reached for a bottom flange with $b_{f,b} = 90$ mm and $t_{f,b} = 40$ mm (corresponding to $b_{f,b}/b_{f,t} = 0.3$), resulting in $M_{cr} = 246$ kNm and $M_{cr,braced} = 906$ kNm for the laterally unsupported beam and the beam braced at midspan, respectively. Further decrease of $b_{f,b}$ (and proportional increase of $t_{f,b}$) is possible to increase the critical bending moment, but negatively impacts the in-plane resistance because then the yield strength of the bottom flange must be reduced [43]. The critical bending moment for the original design ($b_{f,b}/b_{f,t} = 1$) is 128 kNm for the laterally unsupported beam and 738 kNm for the beam braced at midspan. The relative increase of the critical bending moment for the optimised design ($b_{f,b}/b_{f,t} = 0.3$) compared to the initial design ($b_{f,b}/b_{f,t} = 1$) is 93% for the laterally unsupported beam and 23% for the beam braced at midspan.

For $b_{f,b}/b_{f,t}$ ratios > 1 the lateral-torsional buckling resistance decreases. For large ratios $b_{f,b}/b_{f,t}$ a reverse trend is observed, because the comparatively large positive influence of the term $t_{f,t}^3$ on GJ dominates the negative influence of the Wagner effect.

None of the cross-section designs provide sufficient resistance against lateral-torsional buckling in case of the unrestrained beam, because $M_{cr,unbraced} < M_{G,Ed} = 0.125 q_{z,G,Ed} L^2 = 384$ kNm. By providing a brace at midspan the critical bending moment increases to $M_{cr,braced} = 906$ kNm for $b_{f,b} = 90$ mm and $t_{f,b} = 40$ mm($b_{f,b}/b_{f,t} = 0.3$). Taking into account the reduction due to web distortion according to the Dutch National Annex [42] to EN 1993-1-1 [43], it is found that $k_{red} = 0.816$ and $M^*_{cr,braced} = 740$ kNm. The out-of-plane load amplifier is $\alpha_{cr,op} = M^*_{cr,braced}/M_{G,Ed} = 1.93$. The maximum bending stress due to $q_{z,G,Ed}$ is computed, resulting in an in-plane load amplifier $\alpha_{ult,k} = 2.50$. The non-dimensional slenderness $\bar{\lambda}_{op} = 1.14$ and the imperfection factor $\alpha_{LT} = 0.76$ [43] lead to a lateral-torsional buckling reduction factor $\chi_{op} = 0.40$.The final design verification is performed according to Eq. (25) as

$$\frac{\chi_{op}\alpha_{ult,k}}{\gamma_{M1}} = \frac{0.40 \cdot 2.50}{1.00} = 1.0 \geqslant 1.0 \therefore \text{OK} \tag{33}$$

The resistance during execution is therefore sufficient. The maximum normal stress due to $q_{z,G,Ed}$ and $q_{z,Q,Ed}$ is $\sigma = 248$ MPa $< f_y = 355$ MPa and therefore the in-plane bending resistance is also verified.

It should be noted that further design verifications apply in the transient and persistent design situations, either related to resistance (e.g. shear buckling, flange-induced buckling, yielding, etc.) or serviceability criteria. These are not included within the scope of this paper,

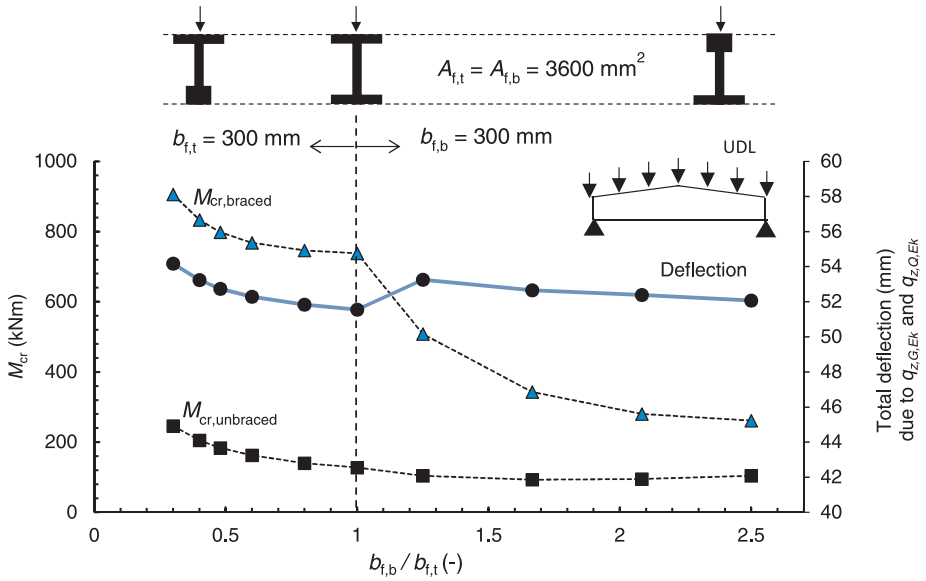

Fig. 6. Critical bending moment and total deflection for the case study demountable composite floor system.

but can be found in the relevant Eurocodes or should be established based on acceptance criteria for reusable structural components.

The total deflection, resulting from $q_{z,G,Ek}$ and $q_{z,Q,Ek}$, does not significantly differ for the range of considered cross-section designs. Compared to the initial design ($b_{f,b}/b_{f,t} = 1$), the maximum increase of the deflection occurs for $b_{f,b}/b_{f,t} = 0.3$, but is only 2.63 mm (5%). The relative increase in deflection is insignificant compared to the substantially larger increase of the critical bending moment for the same cross-sectional area A, implying that the proposed design strategy contributes to efficient material use.

The material efficiency of steel beams could be further considered by the use of high-strength steel (HSS) in the bottom flange [46]. The width of the bottom flange can be reduced proportionally to the relative increase of its yield strength. Local yielding of the web is necessary to utilise the benefits of the high-strength steel bottom flange, which may impair the reusability of the beam due to the associated plastic strain [44]. The reduced area of the bottom flange decreases the distance between the elastic neutral axes of the steel beam and the prefabricated concrete floor elements, leading to a reduced benefit of composite interaction. These considerations indicate that the application of high-strength steel is more challenging in case of reusable steel-concrete composite floor systems compared to the traditional composite floor systems, which are based on plastic design.

6. Conclusion

- Demountable steel-concrete composite floor systems are more sensitive to lateral-torsional buckling compared to monolithic cast in-situ steel-concrete floor systems, mostly because of unsymmetrical loading and the absence of rotational constraints in the execution phase. Lateral-torsional buckling is only relevant during execution; it is prevented by demountable shear connectors in the persistent design situation.
- The Energy method and Rayleigh-Ritz approach were used to develop an analytical prediction model for the critical bending moment of monosymmetrical web-tapered steel beams. The Wagner torsional rigidity was included in the formulation of the internal strain energy, this led to good agreement between the analytical prediction model with finite element results available in literature (max. deviation ± 5%). An overarching strategy to optimise the in-plane and out-of-plane resistance of monosymmetrical web-tapered steel beams was derived. This strategy calls for (i) a comparatively narrow tensile flange compared to the compression flange and (ii) approximately equal area of both flanges. The proposed strategy contributes to efficient material use because the out-of-plane resistance is increased for the same cross-sectional area.
- The optimisation strategy was demonstrated through a case study composite floor system, consisting of a 16 m span simply-supported web-tapered beam and large prefabricated concrete floor elements, connected by demountable shear connectors and loaded by a uniformly distributed load. An initially bisymmetrical cross-section of steel grade S355 was optimised by modifying the bottom flange dimensions from 300 × 12 mm^2 to 90 × 40 mm^2. The critical bending moment increased by 93% and 23% for the laterally unsupported beam and the beam laterally supported at midspan, respectively. The 5% increase of the deflection is considered as insignificant compared to the substantially larger relative increase of the critical bending moment.

Declaration of Competing Interest

The authors declare that they have no known competing financial interests or personal relationships that could have appeared to influence the work reported in this paper.

Acknowledgement

The first author gratefully acknowledges support by the Research Program of the Materials innovation institute (M2i) (www.m2i.nl), supported by the Dutch government, under project number T16045.

The second author gratefully acknowledges the financial support of the Research Fund for Coal and Steel (RFCS), within the research project "Reuse and Demountability using Steel Structures and the Circular Economy" REDUCE (RFCS-02-2015). Cooperation of the project partners (SCI, University of Luxembourg, University of Bradford, Lindab A/S, Tata Steel, Bouwen met Staal and AEC3) is gratefully acknowledged.

References

[1] Organisation for Economic Co-Operation and Development, Global Material Resources Outlook to 2060: Economic Drivers and Environmental Consequences, OECD Publishing; 2019.
[2] United Nations, Decoupling Natural Resource Use and Environmental Impacts from Economic Growth, United Nations Environmental Programme; 2011.
[3] W. Stahel, "The product life factor," An Inquiry into the Nature of Sustainable Societies: The Role of the Private Sector, pp. 72-96, 1982.

[4] Lansink AGWJ. Ladder van Lansink. Dutch Parliamental Procedure 1979.
[5] Danatzko J, Sezen H. Sustainable structural design methodologies. Practice Periodical Struct Design Constr 2011;16(4):186–90.
[6] Worldsteel Association. Sustainable steel: at the core of a green economy. Brussels: Worldsteel Association; 2012.
[7] Fujita M, Iwata M. Reuse system of building steel structures. Struct Infrastruct Eng 2008;4(3):207–20.
[8] Lam D, Dai X, Ashour A, Rehman N. Recent research on composite beams with demountable shear connectors. Steel Constr: Design Res 2017;10(2):125–34.
[9] Moynihan MC, Allwood JM. Viability and performance of demountable composite connectors. J Constr Steel Res 2014;99:47–56.
[10] Wang L, Webster MD, Hajjar JF. Behavior of sustainable composite floor systems with deconstructable clamping connectors. Proceedings of the 8th International Conference on Composite Construction in Steel and Concrete. 2017.
[11] Pathinara SW, Uy B, Mirza O, Zhu X. Flexural behaviour of composite steel-concrete beams utilising blind bolt shear connectors. Eng Struct 2016;114:181–94.
[12] Suwaed ASH, Karavasilis TL. Removable shear connector for steel-concrete composite bridges. Steel Compos Struct 2018;29(1):107–23.
[13] Nijgh MP, Girbacea IA, Veljkovic M. Elastic behaviour of tapered composite beam optimized for reuse. Eng Struct 2019;183:366–74.
[14] Kozma A, Odenbreit C, Braun MV, Veljkovic M, Nijgh M. Push-out tests on demountable shear connectors of steel-concrete composite structures. Structures 2019;21:45–54.
[15] Roberts TM. Finite difference analysis of composite beams with partial interaction. Comput Struct 1985;21(3):469–73.
[16] Lin JP, Wang G, Bao G, Xu R. Stiffness matrix for the analysis and design of partial-interaction composite beams. Constr Build Mater 2017;156:761–72.
[17] Nijgh MP, Veljkovic M. Static and free vibration analysis of tapered composite beams optimized for reuse. Int J Mech Sci 2019;159C:398–405.
[18] NEN, EN 1990: Eurocode 0: Basis of Structural Design, Delft: NEN; 2002.
[19] L. Prandtl, “Kipperscheinungen,” Munich, 1899.
[20] Michell AGM. Elastic stability of long beams under transverse forces. London, Edinburgh, Dublin Philos. Mag J Sci 1899;48(292):298–309.
[21] Snijder HH, Hoenderkamp JCD, Maljaars J. Influence of concrete slabs on lateral torsional buckling of steel beams. Proceedings of the Third International Conference on Structural Engineering, Mechanics and Computation, Cape Town. 2007.
[22] Höglund T. Att konstruera med stål, Läromedel för konstruktörer: Modul 6. Stålbyggnadsinstitutet: Stabilitet för balkar och stänger; 2006.
[23] Nemir MTM. Finite element stability analysis of thin-walled steel structures. Salford: University of Salford; 1985.
[24] Zhang L, Tong GS. Lateral buckling of web-tapered I-beams: A new theory. J Constr Steel Res 2008;64:1379–93.
[25] Benyamina AB, Meftah SA, Mohri F, Daya EM. Analytical solution attempt for lateral torsional buckling of doubly symmetric web-tapered I-beams. Eng Struct 2013;56:1207–19.
[26] Yuan W, Kim B, Chen C. Lateral-torsional buckling of steel web tapered tee-section cantilevers. J Constr Steel Res 2013;87:31–7.
[27] Kitipornchai S, Trahair NS. Buckling properties of monosymmetric I-beams. St. Lucia: University of Queensland; 1979.
[28] Wang CM, Kitipornchai S. On stability of monosymmetric cantilevers. Eng Struct 1986;8(3):169–80.
[29] Soltani M, Asgarian B. Determination of lateral-torsional buckling load of simply supported prismatic thin-walled beams with mono-symmetric cross-sections using the finite difference approach. Amirkabir J. Civil Eng 2018;50(1):23–6.
[30] Trahair N. Lateral buckling of tapered members. Eng Struct 2017;151:518–26.
[31] Asgarian B, Soltani M, Mohri F. Lateral-torsional buckling of tapered thin-walled beams with arbitrary cross-sections. Thin-Walled Struct 2013;62:96–108.
[32] Andrade A, Camotim D, Dinis PB. Lateral-torsional buckling of singly symmetric web-tapered thin-walled I-beams: 1D model vs. shell FEA. Comput Struct 2007;85:1343–59.
[33] Weinstein A. The center of shear and the center of twist. Q Appl Math 1947;5(1):97–9.
[34] Ecsedi I. A formulation of the centre of twist and shear for nonhomogeneous beam. Mech Res Commun 2000;27(4):407–11.
[35] Erkmen RE, Attard MM. Lateral-torsional buckling analysis of thin-walled beams including shear and pre-buckling deformation effects. Int J Mech Sci 2011;53:918–25.
[36] Roberts TM, Azizian ZG. Instability of thin walled bars. J Eng Mech 1983;3:781–94.
[37] Kerensky OA, Flint AR, Brown WC. The basis for design of beams and plate girders in the revised British standard. Proc Inst Civ Eng 1956;5:396–444.
[38] Nethercot DA, Taylor JC. Use of a modified slenderness in the deisgn of laterally unsupported beams. ECCS Colloqium Stability Steel Struct 1977.
[39] Galambos TV. Structural members and frames. Englewood Cliffs: Prentice-Hall; 1968.
[40] Anderson JM, Trahair NS. Stability of monosymmetric beams and cantilevers. J Struct Div 1972;98(1):269–85.
[41] Vensko MJ. Lateral-torsional buckling of structures with monosymmetric cross-sections. Pittsburgh: University of Pittsburgh; 2003.
[42] NEN, EN 1993-1-1 + C2/NB: Dutch National Annex to Eurocode 3: Design of steel structures – Part 1-1: General rules and rules for buildings., Delft: NEN; 2016.
[43] NEN, EN 1993-1-1: Eurocode 3: Design of steel structures – Part 1-1: General rules and rules for buildings, Delft: NEN; 2005.
[44] Steel Construction Institute, “Protocol for reusing structural steel,” Steel Construction Institute, Ascot; 2019.
[45] Zeng X, Jiang SF, Zhou D. Effect of shear connector layout on the behavior of steel-concrete composite beams with interface slip. Appl Sci 2019;9(207).
[46] Veljkovic M, Johansson B. Design of hybrid steel girders. J Constr Steel Res 2004;60:535–47.